Chemical Engineering Journal 410 (2021) 128246

Contents lists available at ScienceDirect

Chemical Engineering Journal

journal homepage: www.elsevier.com/locate/cej

A CFD study of an annular pilot plant reactor for Paracetamol photo-Fenton degradation

Cesar M. Venier [a,d], Leandro O. Conte [b,*], Monserrat Pérez-Moya [c], Moisés Graells [c], Norberto M. Nigro [a], Orlando M. Alfano [b]

[a] Centro de Investigación de Métodos Computacionales (CIMEC), Consejo Nacional de Investigaciones Científicas y Técnicas (CONICET) and Universidad Nacional del Litoral (UNL), 3000 Santa Fe, Argentina
[b] Instituto de Desarrollo Tecnológico para la Industria Química (INTEC), Consejo Nacional de Investigaciones Científicas y Técnicas (CONICET) and Universidad Nacional del Litoral (UNL), 3000 Santa Fe, Argentina
[c] Chemical Engineering Department, Universitat Politècnica de Catalunya, Escola d'Enginyeria de Barcelona Est (EEBE), 08019 Barcelona, Spain
[d] Escuela de Ingeniería Mecánica, Facultad de Ciencias Exactas, Ingeniería y Agrimensura, Universidad Nacional de Rosario, Rosario (UNR), 2000 Rosario, Argentina

ARTICLE INFO

Keywords:
Photo-Fenton
OpenFOAM
Pilot-plant reactor
Radiation model
Paracetamol

ABSTRACT

This work studies in detail the photo-Fenton degradation process of Paracetamol (PCT) on an annular pilot-plant reactor using Computational Fluid Dynamics (CFD). A cylindrical lamp emission model was originally implemented over the structure of the OpenFOAM(R) platform and a multicomponent reaction mixture model was used to compute the temporal evolution of the different species at each point of the reactor. Once the proposed model was experimentally validated, the influence of different operating conditions (i.e. different strategies for hydrogen peroxide (H_2O_2) dosage, use of low recirculation flow rates (Qr), and a completely uncovered lamp setup) was studied. The results of the analysis showed that a double addition of H_2O_2 (50% before the tank and 50% before the reactor) significantly reduces the reaction times of the process. Moreover, the overall PCT degradation rate does not change when Qr is increased, thus allowing the system to be operated with a recirculation flow three times lower than that the one used in the experiments. Thereby, the developed model allows identifying the reaction conditions that maximize the overall PCT conversion, making efficient use of H_2O_2 (main chemical reagent) and reducing the electrical energy consumption (recirculation flow) by operating the system under conditions present in large-scale photochemical reactors.

1. Introduction

The production and consumption of pharmaceutical compounds have been increased considerably in the last years due to the growing use of the world's population. Antibiotics, antipyretics and analgesics are the most widely used drugs. In particular, acetaminophen or paracetamol (PCT) occupy the top of the list among the analgesics [1]. These pharmaceutical compounds, mainly produced from urban and industrial effluents, not properly treated in conventional plants, end up in the environment by different pathways [2–4]. As a consequence, these chemicals and their residues not only have negative impacts on the aquatic ecological systems but have also been detected frequently in drinking waters [5,6], affecting human health [7,8]. Therefore, it is absolutely necessary to develop reliable technologies capable of removing not only the PCT but also its metabolites/degradation products from wastewater prior to being discharged into the environment. Advanced oxidation process (AOPs), are being intensively investigated as a superior alternative to achieve this goal [9–11]. Here, the photo-Fenton process takes advantage due to the high removal efficiencies it shows to remove this type of pollutants, in addition to allowing the use of the sun as a source of energy for the process [12–15]. However, it is known that "traditional" photo-Fenton condition includes acidic medium which means an additional cost for pH adjustment. At this point, the use of iron chelates (such as iron citrate, ferrioxalate, EDDS, etc.) proved to be a surpassing alternative [16–18]. Also, there are several studies in the specific literature regarding the effect of organic and/or inorganic species when the photo-Fenton process is applied in real wastewater [19–21]. Nevertheless, it should be noted that all these topics have been studied using ideal reactor models.

The efficient implementation of these AOPs involves the resolution of multi-component, non-ideal reactor models, which consists of computing the spatial distribution of the reacting species and the

* Corresponding author.
E-mail address: lconte@santafe-conicet.gov.ar (L.O. Conte).

https://doi.org/10.1016/j.cej.2020.128246
Received 3 July 2020; Received in revised form 20 November 2020; Accepted 18 December 2020
Available online 25 December 2020

evaluation of the radiation field inside the reactor. Computational Fluid Dynamics (CFD) meets these requirements and can be used as a powerful cost-effective tool to improve the reactor design and optimize operations by modelling all relevant phenomena, without the need to carry out large amounts of experimental testing [22–24]. Besides, these simulations can improve the system performance maximizing the reaction efficiency and yield, while minimizing the reagent and energy consumption in large-scale reactors. Although there are works where AOPs are analysed using computational approaches [25–27], at present, there is still a lack of assessment and discussion in the literature on the modelling of the photo-Fenton processes using pilot plant-reactors with explicit radiation absorption effects via CFD techniques.

Therefore, the main objective of this research is to develop a full CFD model for the PCT photo-Fenton degradation process using an annular pilot-plant photoreactor, which includes the high non-uniformity of the radiation field and therefore of the reactive species involved in the chemical process. In addition, the model is used to study the system behaviour for operating conditions normally present in large-scale photochemical reactors (not perfect mixing conditions, different setups for oxidant agent dosage and lamp irradiation requirements). Moreover, complete modelling of the system and its FVM mesh, a set of pre and post-processing techniques, an induced pressure loss (hydraulic pump) and an efficient method for averaging fields over different sections of the domain is included. Here, the open-source platform OpenFOAM(R) v7 [28] based on the Finite Volume Method (FVM) is used to develop a complete 3D model of the system over the general structure of the `reactingFoam` solver. This code has the capability of solving a set of species balance equations along with the transient mass and momentum balances. However, while its performance for combustion phenomena has been reported extensively in the literature [29–31] there is still a lack of assessment for other applications, such as isothermal reaction phenomena. After verifying the CFD results against the experimental data, the study focuses on the influence of different operational conditions on the system's efficiency, which cannot be done otherwise by analytical approaches. In this regard, CFD combined with experimental measurements is the current trend to give a complete and thorough insight into the physical and chemical phenomena.

2. Materials and methods

2.1. Experimental setup

Fenton and photo-Fenton assays were performed in a 15 L pilot plant reactor (see Fig. 1). The device is composed by a jacketed glass reservoir tank (9 L) and an annular photoreactor (two concentric borosilicate cylinders, 6 L) equipped with an Actinic lamp Philips BL TL-DK 36W/10 1SL; the illuminated volume is only 10% of the total volume (1.5 L). The incident photon power, $E = 3.36 \times 10^{-4}$ E min^{-1} (300 to 420 μm) was measured using potassium ferrioxalate actinometry [32]. Also, the system is equipped with a recirculation pump with a flowmeter, a pH sensor and a thermostatic bath for the temperature control. Further details of the reaction system and experimental protocol can be found in Audino et al. [33].

To assess the applicability of the Fenton and photo-Fenton processes in highly contaminated paracetamol wastewater, such as effluents from pharmaceutical industries, a concentration of 40 mg L^{-1} was studied [34–36]. For this initial concentration of the contaminant, the stoichiometric dose of oxidant agent (Hydrogen Peroxide, H_2O_2) to achieve its total mineralization was 189 mg L^{-1}. Furthermore, the maximum value of the initial concentration of Fe^{+2} (10 mg L^{-1}) was set taking into account the maximum legal value in wastewaters in Spain [37]. Therefore, for the design of experiments, three H_2O_2 concentration levels (half and twice the stoichiometric dose, 94.5, 189 and 378 mg L^{-1}) and Fe^{+2} concentration (5, 7.5 and 10 mg L^{-1}) were used.

Regarding the experimental procedure, the reservoir tank was filled initially with 10 L of distilled water and then, 4.9 L of distilled water in which PCT was previously dissolved, were added. Once pH was adjusted to 2.8 ± 0.1, the remaining 0.1 L of distilled water in which Fe^{+2} was previously dissolved, were filled and the light was switched on (for irradiated conditions). Finally, H_2O_2 was added at the sampling point (see Fig. 1). The recirculation flow rate (Qr) was set to 12 L min^{-1} (Re = 1820, laminar flow) [32]. During these experiments, pH and temperature were continuously monitored to remain in the range of 2.8 ± 0.2 and 25.0 ±2.0 °C, respectively. The total reaction time was fixed to 120 min.

2.2. Analytical determination

Measurements of PCT (>98% purity, Sigma-Aldrich, USA), hydrogen peroxide (H_2O_2, Panreac Química SLU, Spain) and iron species concentrations were carried out during the experiments. PCT was determined using an HPLC Agilent 1200 series with UV-DAD at 243 ηm and the samples were pre-treated with methanol (>99,9% purity, J.T. Baker Inc., USA) to stop the Fenton reaction. The concentrations of H_2O_2 and iron species ([Fe^{+2}], [Fe^{+3}], [$Fe^{[TOT]}$]) were determined with a UV–VIS spectrometer following standard methods [38,39]. Further details of the experimental measurement procedure and its errors can be found in the work of Yamal-Turbay et al. [32].

3. Computational methodology

In this work, CFD simulations are performed with the open-source software OpenFOAM(R) v7 [28], particularly using an adapted version of the `reactingFoam` solver. The code addresses a discretized form of the mass, momentum and energy balance equations based on the collocated Finite Volume Method (FVM) and the coupling between equations is achieved using a segregated algorithm of the SIMPLE family [40,41]. In the same process, a species transport balance (one for each component present) is solved where the reaction term of each one of these equations is obtained separately from an external system of ODEs.

3.1. Balance equations

To obtain the spatial and temporal distribution of the concentration of each species present in the mixture, the FVM discretized form of the mass and momentum balances are solved for the multicomponent mixture. The viscosity and density of liquid water are used for solving these equations, since it is, by far, the main component of the mixture (>99%). Therefore, the mixture is modelled as a homogeneous medium using the same set of balance equations in the whole domain to obtain the pressure and velocity fields, as well as the concentration of each species at each point in time and space. The proposal is to decouple the mass and momentum balance from the species balance. In this way, first, the flow is computed for steady-state conditions. Then, the concentration of each component is obtained based on solving the species balance equations using the velocity and pressure obtained previously. This manipulation can be done on the basis that the flow is mainly steady according to the experimental observations.

The transport equation for each species in the mixture is given by Eq. (1).

$$\frac{\partial Y_i}{\partial t} + \vec{\nabla} \cdot (\vec{u}\, Y_i) = \vec{\nabla} \cdot (D_i\, \vec{\nabla} Y_i) + r_i \tag{1}$$

Here, $\vec{u}$ represents the velocity field of the mixture, D_i is the diffusivity of the i-component on water and Y_i is the concentration of the i-component. The r_i term is the source of the i-species given by the chemical reactions involving those species.

To determine these r_i terms, a system of ODEs is solved to account for the chemical reactions involved at each time step. Here, the kinetic

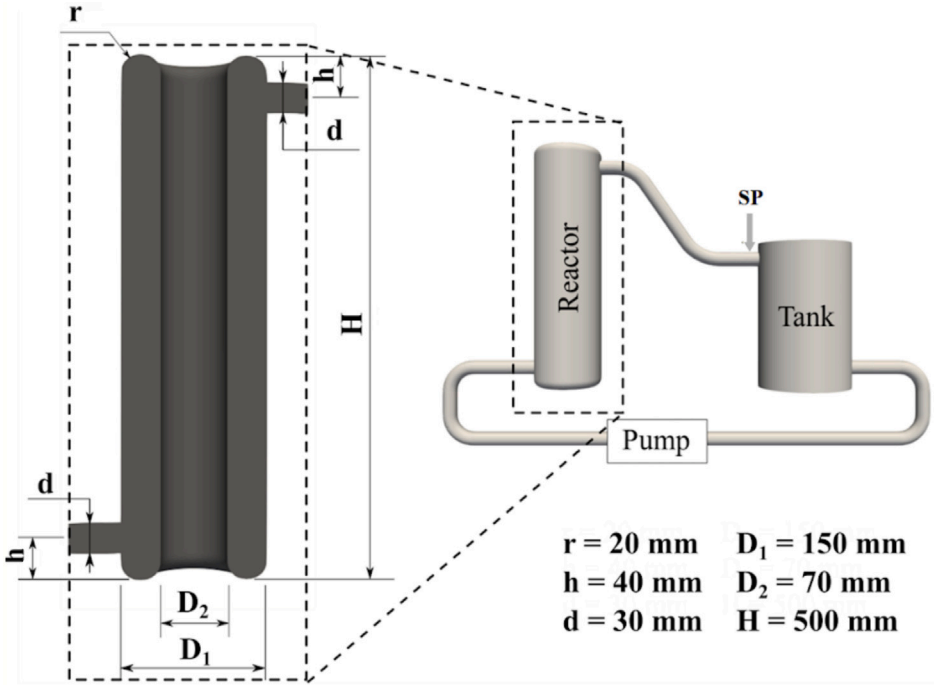

Fig. 1. Sketch of the reacting system (right) and a vertical plane cut over the annular reactor (left). Experimental Sampling Point (SP).

constants accounting for Fenton and Fenton-like reactions, and the hydroxyl radical attack to H_2O_2 and PCT were taken from the work of Audino et al. [33]. The reaction rates expressions obtained for the reactive species PCT, H_2O_2, Fe^{+2}, Fe^{+3} and radicals consider, on the one hand, the thermal (Fenton) reaction rate taking place in the total volume of the system and, on the other, the irradiation-activated (photo-Fenton) reaction occurring inside the irradiated liquid volume.

3.2. Radiation model

The radiation field evaluation is crucial for a correct photoreactor design, analysis and optimization. Specifically, the radiation field expressed in terms of the Local Volumetric Rate of Photon Absorption (LVRPA) can be introduced into kinetic expressions, thus obtaining the photochemical reactions rate equations. Starting from the Radiative Transfer Equation (RTE) [42,43], and assuming: (i) steady-state conditions of the radiation field, (ii) no radiation emission and (iii) homogeneous medium (only radiation absorption), the LVRPA can be computed by solving Eq. (2).

$$e^a_\lambda(\vec{x},t) = \kappa_\lambda \int_\Omega I_\lambda(\vec{x},\vec{\Omega},t)d\Omega \tag{2}$$

where I_λ is the spectral radiation intensity, Ω is the solid angle and κ_λ the spectral volumetric absorption coefficient.

There are several approaches to determine the radiation intensity, from solving the complete Radiation Transport Equation (RTE) to modelling I_λ based on different assumptions and simplifications. The advantages and drawbacks of these approaches have been discussed in the literature [44]. For the system under study, the effects of radiation scattering and emission inside the reactor are negligible, which allows the direct use of the RTE analytical solution. Taking into account the hypotheses made by Irazoqui et al. [45] for a tubular lamp with uniform surface emission in space and isotropic in all directions, the radiation intensity is given by Eq.(3).

$$I_\lambda(\vec{x},\theta,\phi,t) = \frac{\Gamma_{R,\lambda}P_\lambda}{2\pi^2 R_L L_L} \exp\left[-\int_{\bar{s}=s_R}^{\bar{s}=s(\vec{x},\theta,\phi)} \kappa_\lambda(\bar{s},t)d\bar{s}\right] \tag{3}$$

where $\Gamma_{R,\lambda}$ is the reactor wall transmission coefficient, P_λ the output power provided by the lamp, and R_L and L_L are the radius and length of the lamp, respectively. The limits of the integration variables θ and φ can be obtained from trigonometric relationships [46].

Thus, incorporating Eq. (3) in Eq. (2), the value of the LVRPA at any point inside the reactor and at any time for a single wavelength can be computed based on Eq. (4).

$$e^a_\lambda(\vec{x},t) = \frac{\kappa_\lambda(\vec{x},t)P_{\lambda,s}}{2\pi^2 R_L L_L} \int_{\phi_1}^{\phi_2}\int_{\theta_1}^{\theta_2} \sin(\theta)\exp\left[-\int_{\bar{s}=s_R}^{\bar{s}=s(\vec{x},\theta,\phi)} \kappa_\lambda(\bar{s},t)d\bar{s}\right] d\theta d\phi \tag{4}$$

For cases where polychromatic radiation source is used, an integration of Eq. (4) for the entire range of useful wavelengths is necessary. Then, the radiation field in every point of the reactor, expressed in terms of the LVRPA, is introduced into kinetic expressions (photochemical reactions).

Fig. 2 shows the spatial distribution of the LVPRA in the annular photoreactor. Here it can be seen that, although only a fraction of the lamp is uncovered (130 mm), each point in the photoreactor is irradiated with different intensities (Fig. 2.b). The maximum photon absorption of the liquid mixture is given at an axial position where the lamp is uncovered (0.185 m < z < 0.315 m) and in the proximity of the outer wall of the inner cylinder of the reactor. The result of including Eq. (4) gives an exponential decay of the radiation field (and photon absorption) with the position respect to the lamp (Fig. 2.b and .c).

3.3. Numerical approach and setup

The simulation of the photo-Fenton process (as described in Fig. 3) consists on drawing and meshing the system given in Fig. 1, solving (i) the steady-state momentum equations to obtain the flow, the transient species balance for each component taking into account the kinetic constants of each reaction and the LVRPA at each point of the reactor; and (ii) postprocessing of the results.

The system domain is discretized in hexahedral and tetrahedral cells using the `snappyHexMesh` tool of the OpenFOAM suite. To optimize computer resources while maintaining a satisfactory accuracy of the results, a mesh convergence study was carried out. Different refinements were evaluated, and the coarser grid for which the solutions present

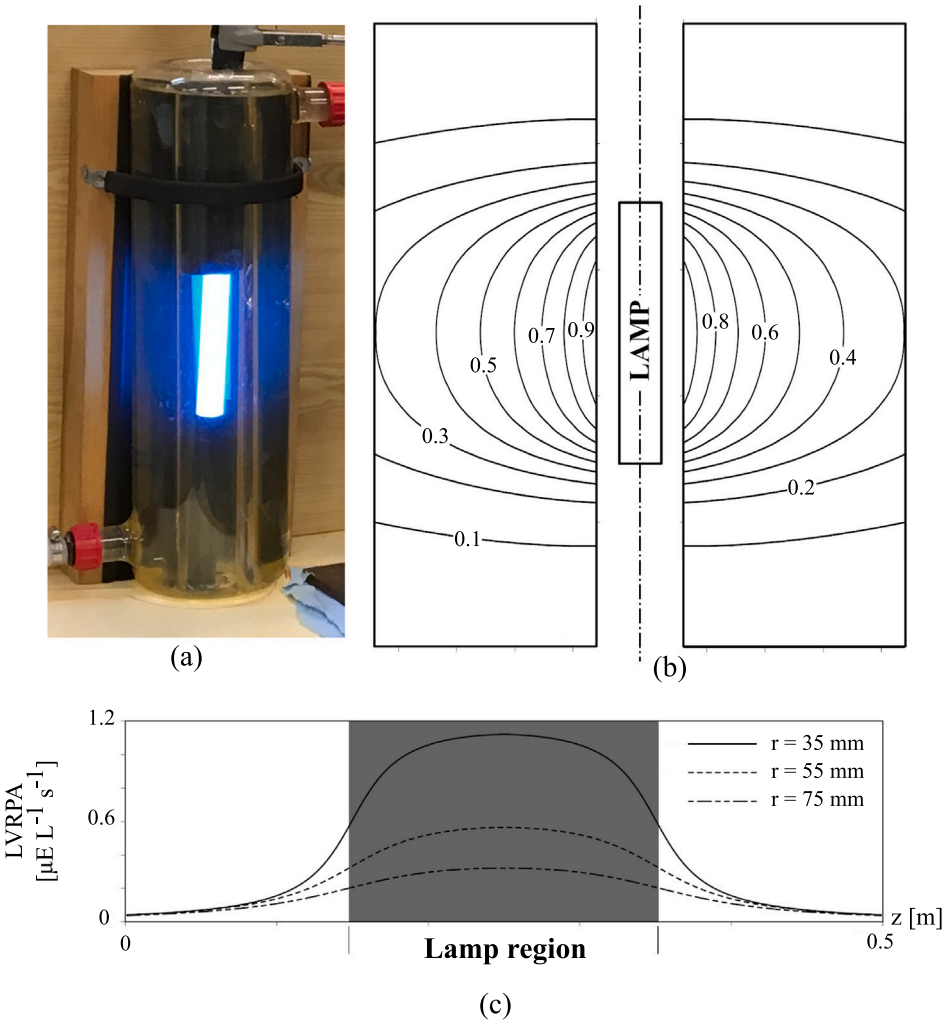

Fig. 2. (a) Photograph of the pilot plant reactor; (b) Isocontour lines of LVRPA on a schematic vertical mid plane of the reactor with coefficients at each contour line representing the normalized LVRPA (over its maximum value: 1.2 μE L^{-1} s^{-1}); (c) LVRPA as a function of the reactor height for different radial positions. Irradiated height: 130 mm. Fe^{+3} = 5 mg L^{-1}.

a relative difference in the velocity field values of less than 1% was adopted (877.758 cells). The details of the FVM grid can be observed in Fig. 4.

The boundaries of the domain (i.e. the glass walls of the reactor, the tubes connecting each part of the system and the tank) are walls with no-slip conditions for the flow, while, for each species, the composition at these boundaries is considered to have a null gradient. The recirculation of the mixture is obtained by a pump that is modelled by a set of FVM cells with a fixed pressure gradient located in the tube before the reactor inlet (see Fig. 4).

The system is simulated for different operational conditions: (i) using increasing recirculation flow rates (Qr) 2, 4, 7 and 12 L min^{-1}, (ii) setting different setups for a single localized injection of the oxidant agent H_2O_2: (A) 100% before the tank, (B) 100% before the reactor and (C) 50% before the tank and 50% before the reactor; and (iii) two lamp operating conditions (partially covered or completely uncovered). The different types of H_2O_2 injection (microlitres of oxidant added into a specific place of the reactor) were always done by considering the overall concentration of H_2O_2 used over the total reaction volume (15 L).

4. Results and discussion

4.1. CFD model analysis and experimental verification

As mentioned before, the simulations tests are segregated in two parts. First, the mass and momentum equations are solved to obtain a steady-state flow in the whole domain by considering that every boundary acts as a wall condition. Then, a uniformly distributed amount of reacting components is incorporated in the system but not for the H_2O_2, so no process reaction can be initiated. The oxidant agent is then injected in fixed locations as previously described, which will be carried through the whole system by the pre-established flow. Simultaneously, the multiple reactions of the photo-Fenton process will occur as the different species recirculate over the system.

Snapshots on vertical cutting planes of a typical CFD simulation of the system may be appreciated in Fig. 5. Here, the concentration of PCT, H_2O_2 and Fe^{+3} after 50 s since the oxidant agent injection (using setup C) is shown. Fig. 6 presents three-dimensional views of the inside of the reactor, showing the LVRPA field distribution for partially covered lamp (Fig. 6.a) and completely uncovered lamp (Fig. 6.b).

Fig. 7 shows the grid refinement inside the reactor and the vertical component of the velocity at left and the PCT concentration during the

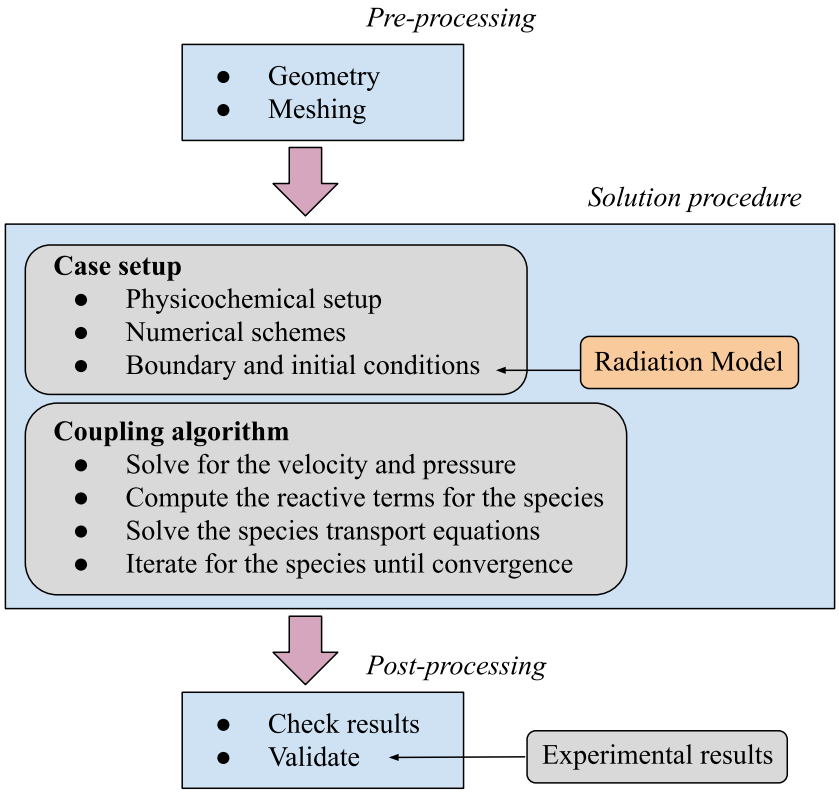

Fig. 3. Scheme of the algorithm.

degradation process at right. Here, a higher level of refinement near the walls of the reactor can be observed, which produces a smooth variation of the velocity field capturing the hydrodynamic boundary layer.

In Fig. 8, the comparison between experimental and predicted concentrations of H_2O_2 and PCT obtained for dark (Fig. 8.a) and irradiated conditions (Fig. 8.b) is shown (Qr = 12 L min^{-1}). First, it is important to highlight the good fit obtained from the experimental data using CFD model (continuous lines). In this regard, the root-mean-square error (RMSE) resulted in 0.68 mg L^{-1} and 8.40 mg L^{-1} for PCT and H_2O_2, respectively, which are less than the errors of the corresponding experimental measurements. Moreover, these results are very close to those obtained considering the system as a perfect mixing reactor (dashed lines), where the RMSE between model and experiment is 0.55 mg L^{-1} for PCT and 8.65 mg L^{-1} for H_2O_2. It is also observed that the irradiated condition (Fig. 8.b) led to the complete PCT removal in only 150 s (minimum degradation time observed). For dark conditions and the minimum concentration of oxidizing agent (H_2O_2 = 94.5 mg L^{-1}) and catalyst (Fe^{+2} = 5 mg L^{-1}), the reaction time necessary to achieve complete PCT destruction is increased 300% (maximum degradation time observed).

After the CFD comparisons against experiments, different operating conditions were simulated, which are discussed in the following sections. For this analysis, the reaction settings with the greatest practical interest were selected. That is, using the lowest concentration of the oxidizing agent, H_2O_2 = 94.5 mg L^{-1} (the most expensive reactant), the highest concentration of catalyst allowed, Fe^{+2} = 10 mg L^{-1} (DOGC, 2003), and a fully uncovered lamp setup (500 mm).

4.2. Local PCT consumption

This section focuses on the concentration of reactants at different heights in the annular reactor and its evolution over time. To simplify the analysis, the local concentration of each component is presented as a function of time and the axial position inside the reactor by taking area-weighted averages on many horizontal cutting planes in the reactor. Fig. 9 shows the spatial and temporal evolution of PCT and H_2O_2 for injection setups A, B and C, respectively.

Fig. 9.a shows that before 50 s of H_2O_2 injection, PCT consumption occurs only in the lower part of the reactor. This may be explained by considering that, due to the low recirculation flow rate, the oxidant agent has not reached the upper part of the reactor yet (Fig. 9.b). Only after 100 s, the PCT degradation is taking place inside the whole reactor. Moreover, to reach a local PCT concentration lower than 1 mg L^{-1} (experimental quantification limit) in the reactor, at least 300 s are needed.

Fig. 9.c shows that, when the injection is made before the reactor, around 325 s are needed to reach the 1 mg L^{-1} limit of PCT concentration. Here, an excess of oxidant agent (as shown in Fig. 9.d where the concentration of H_2O_2 is up to 425 mg L^{-1} at 50 s of operation) produces a scavenging effect, consuming hydroxyl radicals and decreasing PCT degradation rate.

By making the dual injection of oxidant agent (setup C), the local concentration of PCT reaches values below 1 mg L^{-1} after 250 s (Fig. 9.e). This time is 30% less than the time needed with setup B. It is important to remark the more uniform distribution of the oxidant agent inside the reactor (between 50 and 215 mg L^{-1}), which allows a homogeneous degradation of PCT. This reduces the unnecessary consumption of the reagent (reaction of self-decomposition and hydroxyl radical consumption). These behaviours may be extended for higher recirculating flow rate conditions, where it has been seen that for Qr = 4 L min^{-1}, at least 235 s are still needed to obtain local PCT concentrations below 1 mg L^{-1} in all sections of the reactor (results not shown). For higher flow rate conditions (Qr = 7 L min^{-1}), the injection setup has a negligible effect on the required time to reach the PCT concentration criteria (225 s). However, the concentration of PCT at different heights inside the reactor might be affected. Fig. 10 shows the PCT concentration difference between the outlet and the inlet of the reactor for injection setups A and C. The distribution for setup A is highly uneven inside the reactor in the first 100 s from the injection

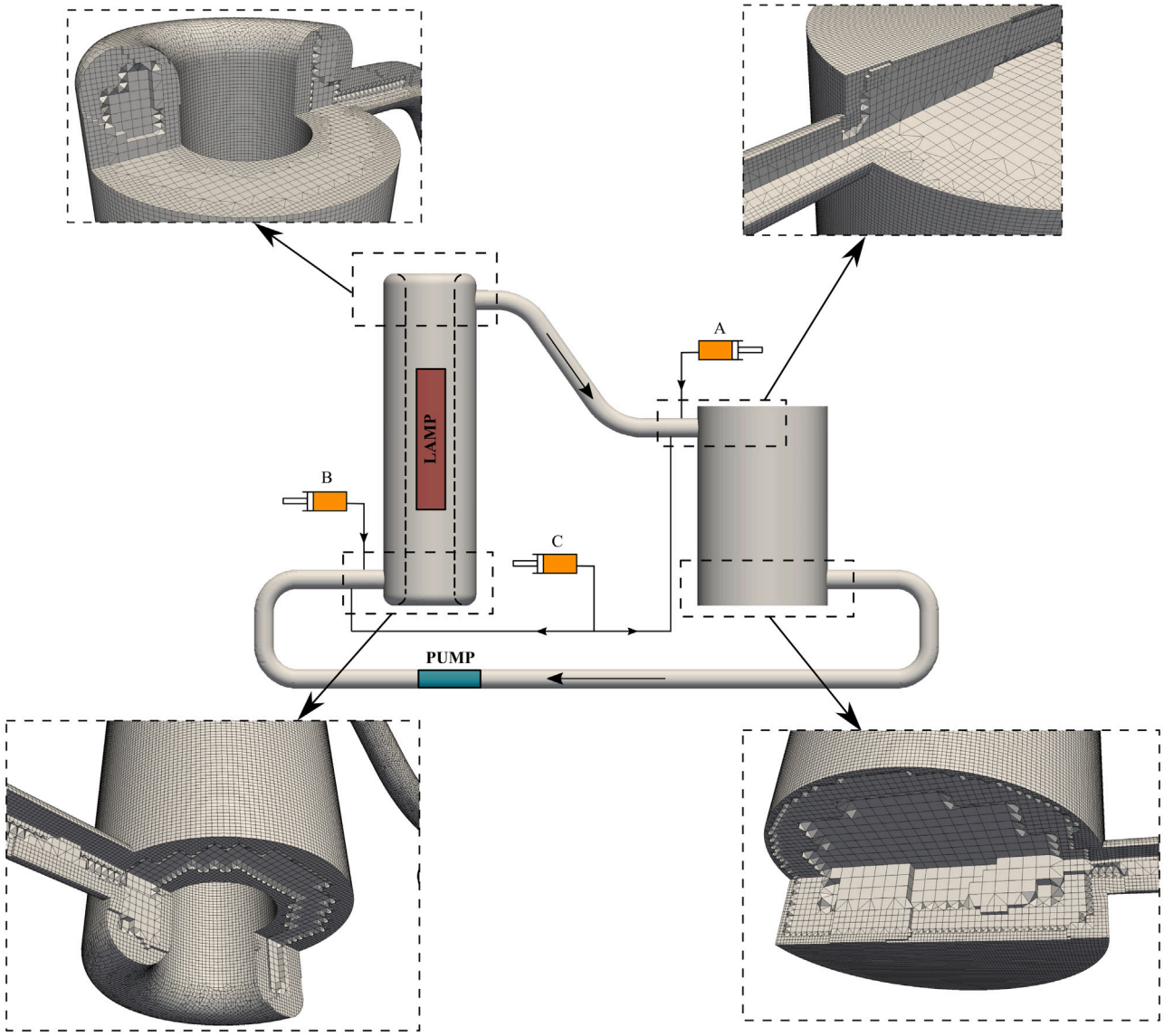

Fig. 4. CFD domain of the system and the FVM mesh.

time. For example, 50 s after the injection, the difference for setup A is ~13 mg L^{-1}, with a PCT concentration leaving the reactor around 30 mg L^{-1}. On the other hand, for setup C this difference is less than 1 mg L^{-1}, with a PCT concentration leaving the reactor of 13.5 mg L^{-1} and almost constant in the whole reactor.

4.3. Overall PCT consumption

The previous analysis showed the effects of different conditions on the local consumption of PCT in the system. However, nothing is said regarding the different reactions and consumption/production rates of different chemical compounds on the whole system (reactor and tank). In this section, the transient evolution of the volume-averaged PCT over the whole domain is evaluated. This allows drawing some conclusions and recommendations about the general behaviour of the system.

Fig. 11 shows the transient evolution of the volume-averaged PCT concentration. This was done for the 3 types of injections previously described (setups A, B and C) and for a recirculation flow rate of Qr = 2 L min^{-1}. The comparison between setups shows that the most effective way of injecting the reactant, in terms of reaching an overall PCT concentration below 1 mg L^{-1} in the shortest possible time is setup C (t = 250 s). This time is 30% less than the time needed with setup B. For this condition, the global behaviour of the system is similar to the local results obtained in the reactor. These results indicate that it is important to inject at least part of the reactant before the tank. This may be attributed to the high residence times, which allows the H_2O_2 to be in contact with the PCT for longer periods without being dragged by the flow.

The effect of using different recirculation flows (Qr = 2, 4, 7 and 12 L min^{-1}) is shown in Fig. 12. Here, the graphic shows the different curves of PCT concentration for each flow considered along with an inserted table showing the temporal evolution of PCT conversion. For injection setup C, the recirculation flows considered do not seem to produce a significant impact on the volume-averaged PCT consumption rate. However, the condition of Qr = 2 L min^{-1} requires 20 s more than the rest of the conditions to reach the PCT concentration criteria. This analysis shows that using a dual injection of the oxidant agent, the system can operate with a recirculation flow (Qr = 4 L min^{-1}) three times lower than the one employed experimentally (Qr = 12 L min^{-1}). This implies a significant reduction in energy consumption by the system.

Finally, the post-processing of the complete system indicates that for high recirculating flows (above 4 L min^{-1}) and with a dual injection of H_2O_2 (setup C), a uniform distribution of reactants is achieved very

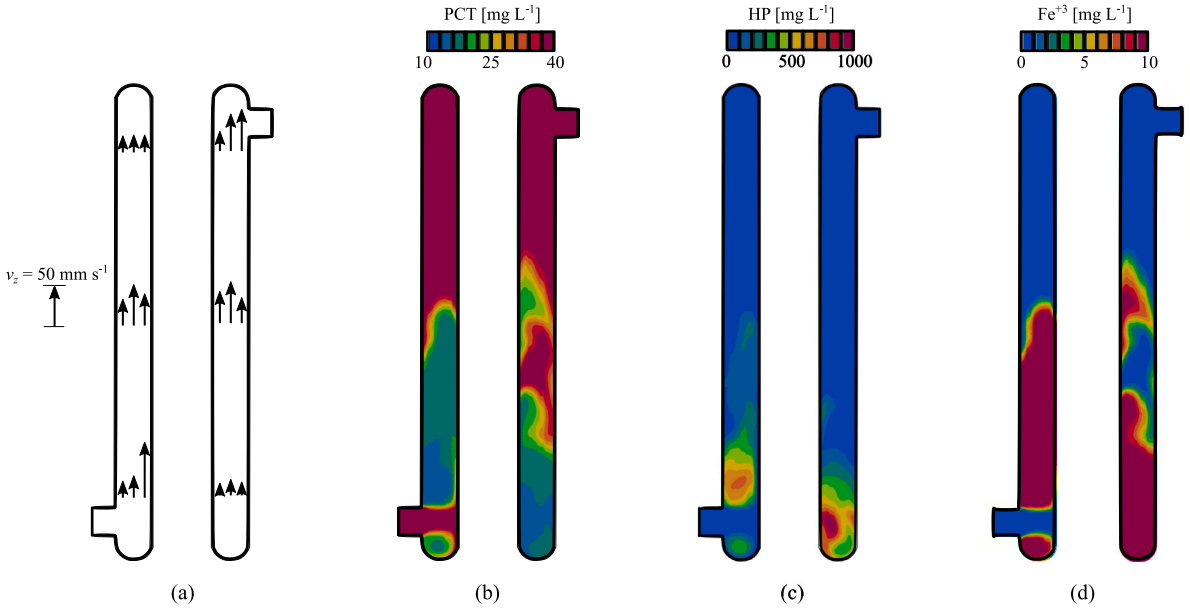

Fig. 5. Qualitative description of the velocity field and species concentration at a central cutting plane after 50 s with injection setup C: (a) velocity vectors, (b) PCT concentration, (c) H_2O_2 concentration and (d) Fe^{+3} concentration. Qr = 2 L min^{-1}; H_2O_2 = 94.5 mg L^{-1}; Fe^{+2} = 10 mg L^{-1}.

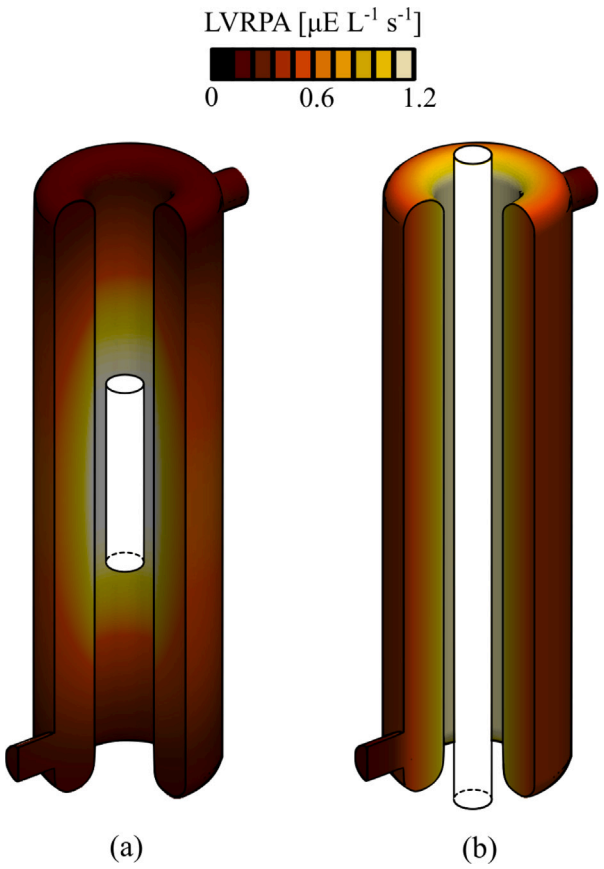

Fig. 6. Radiation field for different lamp operating conditions: LVRPA field for (a) the lamp partially covered and (b) the lamp completely uncovered. Fe^{+2} = 10 mg L^{-1}.

quickly in the system. Therefore, for the evaluated reactions conditions, the concentration of each component depends on the time almost exclusively and the acceleration of reactions given by the lamp radiation (photo-Fenton effect) is not significant.

5. Conclusions

The numerical simulation of the Paracetamol (PCT) photo-Fenton degradation process computing the LVRPA in every point of an annular

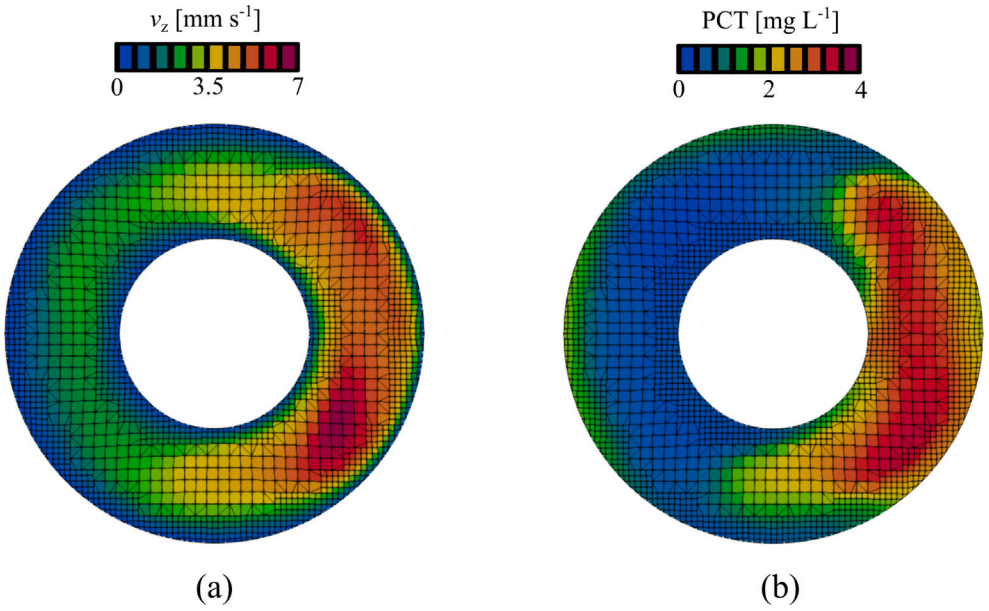

Fig. 7. Horizontal cutting planes inside the reactor at z = 400 mm and after 200 s showing the FVM grid with: (a) the z-component of the velocity and (b) the PCT concentration. Qr = 2 L min^{-1}; H_2O_2 = 94.5 mg L^{-1}; Fe^{+2} = 10 mg L^{-1}.

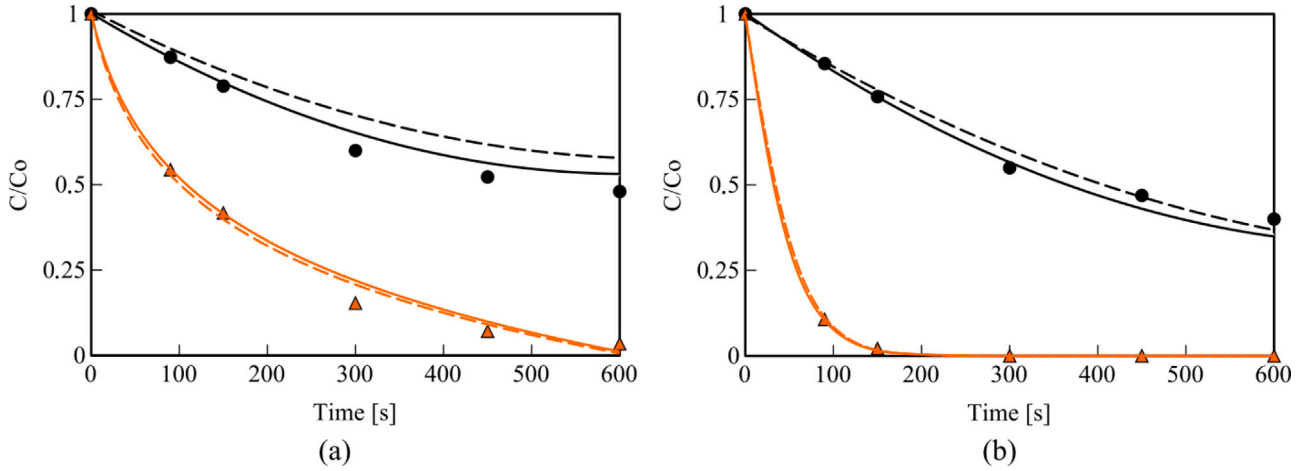

Fig. 8. Experimental concentrations of PCT (triangles) and H_2O_2 (circles), and predicted concentrations of PCT (orange) and H_2O_2 (black) for Qr = 12 L min^{-1}. (a) Fe^{+2} = 5 mg L^{-1}; H_2O_2 = 94.5 mg L^{-1}; dark condition, and (b) Fe^{+2} = 10 mg L^{-1}; H_2O_2 = 378 mg L^{-1}; irradiated height: 130 mm.

pilot-plant reactor was carried out using an open-source CFD platform OpenFOAM(R). For this, a full 3D model of the system which includes the high non-uniformity of the radiation field, and therefore of the reactive species involved, was developed and experimentally validated.

A good agreement was obtained between the experimental data and the CFD model predictions for dark and irradiated conditions for high flow rates (Qr = 12 L min^{-1}). Moreover, these results are very close to those obtained considering the system as a perfect mixing reactor. Using a partially uncovered lamp setup, a complete PCT removal was obtained after 150 s from the injection of the oxidant agent (at the maximum reaction rate conditions according to the experiments: H_2O_2 = 378 mg L^{-1} and Fe^{+2} = 10 mg L^{-1}). Conversely, for dark conditions and considering the minimum concentration of oxidizing agent (H_2O_2 = 94.5 mg L^{-1}) and catalyst (Fe^{+2} = 5 mg L^{-1}), the reaction time necessary to achieve a complete PCT consumption was increased 300% (maximum degradation time required according to the experiments).

After the verification of the code, the system was analysed under different operating conditions. That is, localized additions of the oxidizing agent (H_2O_2), use of low recirculation flow rates (Qr), and a completely uncovered lamp setup. Here, the local and overall PCT degradation rates were evaluated using a lowest concentration of oxidizing agent (H_2O_2 = 94.5 mg L^{-1}), the highest concentration of catalyst allowed (Fe^{+2} = 10 mg L^{-1}) an uncovered lamp (500 mm irradiated length). Using low recirculation rates (Qr = 2 L min^{-1}) and injecting the H_2O_2 before the reactor, up to 325 s of reaction time was required to reach a PCT concentration of less than 1 mg L^{-1} inside the reactor. Here, an excess of oxidant agent (concentration of H_2O_2 is up to 425 mg L^{-1} at 50 s of operation) produces a scavenging effect, consuming hydroxyl

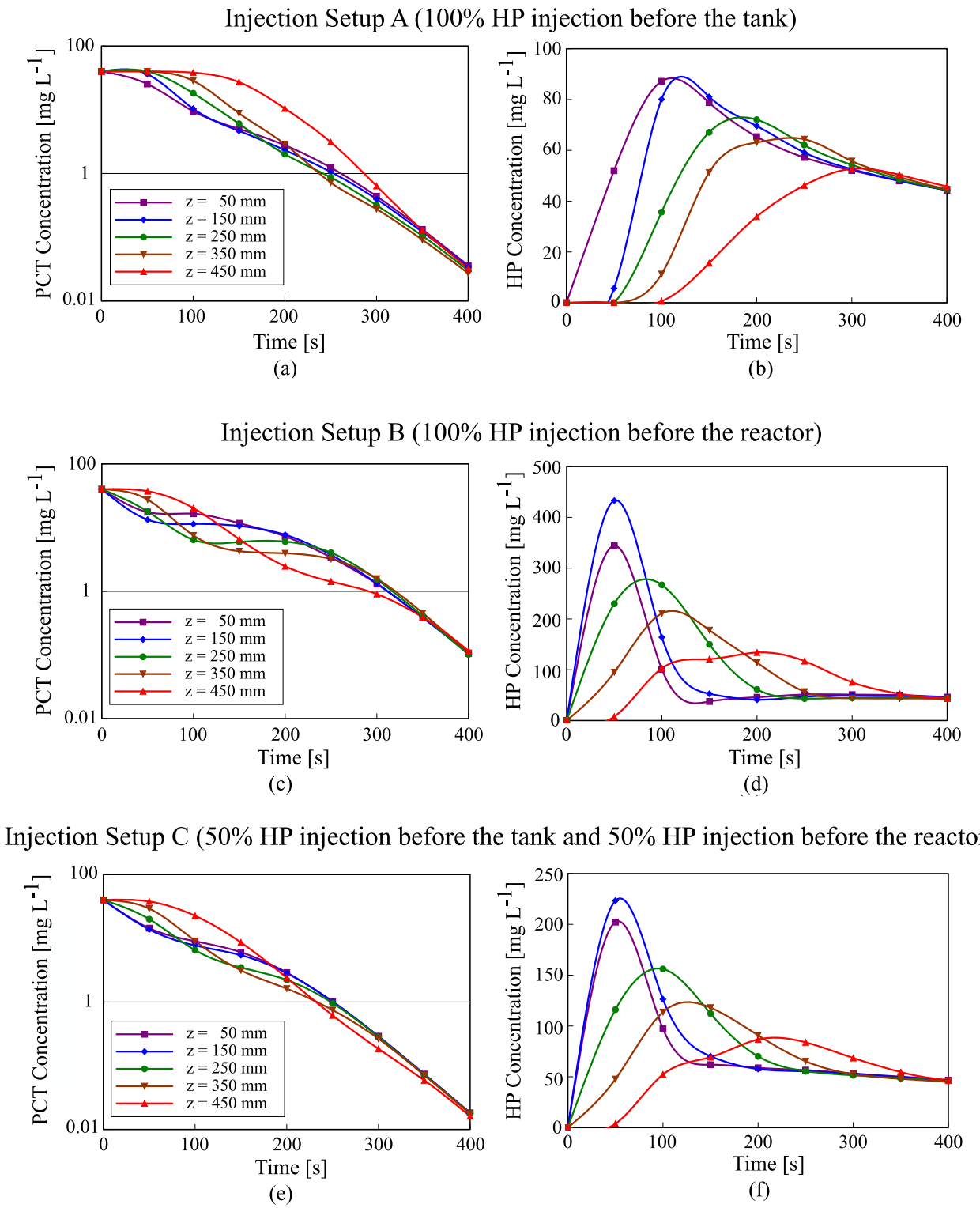

Fig. 9. PCT and H_2O_2 time evolution along the vertical axis of the reactor with Qr = 2 L min^{-1} for Fe^{+2} = 10 mg L^{-1} and H_2O_2 = 94.5 mg L^{-1}: (a) PCT (in semi log scale) with injection setup A, (b) H_2O_2 with injection setup A, (c) PCT (in semi log scale) with injection setup B, (d) H_2O_2 with injection setup B, (e) PCT (in semi log scale) with injection setup C and (f) H_2O_2 with injection setup C.

radicals and decreasing PCT degradation rate. However, making a dual injection of H_2O_2 (50% before the reactor and 50% before the tank), the local PCT concentration reached the threshold of 1 mg L^{-1} after 250 s. Moreover, it produced a more uniform distribution of the oxidant agent inside the reactor (between 50 and 215 mg L^{-1}) allowing a homogeneous degradation of PCT and reducing the unnecessary consumption of the reagent. This behaviour could be extended for higher recirculating flow conditions (Qr > 4 L min^{-1}).

Regarding the overall PCT degradation rate in the system, it was shown that the dual H_2O_2 injection was the most effective way (1 mg

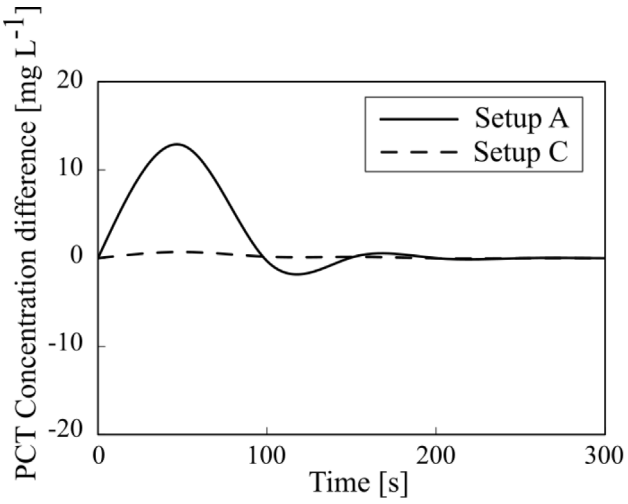

Fig. 10. Difference between the concentration of PCT at the reactor outlet for injection setups A and C with Qr = 7 L min^{-1} for Fe^{+2} = 10 mg L^{-1} and H_2O_2 = 94.5 mg L^{-1}.

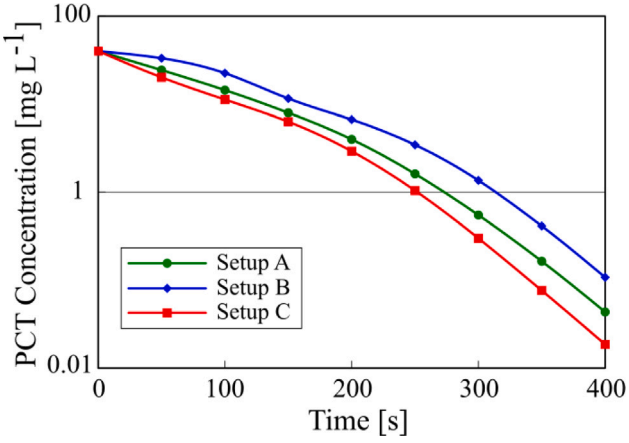

Fig. 11. Temporal evolution of the volume-averaged PCT on the system for different injection setups using Qr = 2 L min^{-1} for Fe^{+2} = 10 mg L^{-1} and H_2O_2 = 94.5 mg L^{-1}.

L^{-1} of PCT in 250 s) of injecting the reactant, for the low recirculation rate (Qr = 2 L min^{-1}). The time required to reach this goal was 30% less than the time needed by making a single H_2O_2 injection after the reactor. In this sense, the global behaviour of the system was similar to the one observed locally in the reactor. For both approaches, the results indicated that it is important to inject part of the reactant before the tank to reduce the reaction times. Moreover, for the dual H_2O_2 injection setup, the higher recirculation rates considered (from 4 to 12 L min^{-1}) did not produce a relative impact on the overall PCT conversion. Although the maximum flow rate (12 L min^{-1}) produced the fastest consumption, the difference between the alternatives is marginal. Therefore, the system could be operated with a recirculation flow rate (Qr = 4 L min^{-1}) three times lower than that used in experimental laboratory tests (Qr = 12 L min^{-1}).

The results show that the proposed CFD model allows identifying the operating conditions that maximize the performance of the system (PCT degradation rate) minimizing the reagent consumption (hydrogen peroxide) and electrical energy costs of the recirculation pump. Therefore, CFD-aided modelling can be used as a robust tool for the design of a new facility or the optimization of existing large-scale photochemical reactors. This allows to enhance the performance, reducing time, costs and manpower without the need to carry out many experimental tests.

Declaration of competing interest

The authors declare that they have no known competing financial interests or personal relationships that could have appeared to influence the work reported in this paper.

Acknowledgements

This work was supported by Ministerio de Economía, Industria y Competitividad (MINECO) and European Regional Development Fund (AIMS, DPI2017-87435-R) of Spain; and Universidad Nacional del Litoral (UNL, CAI+D 50420150100009LI, CAI+D PJ 0020150100093LI and CAI+D PIC 50420150100067LI), Consejo Nacional de Investigaciones Científicas y Técnicas (CONICET, PIP-2015 0100093), Universidad Nacional de Rosario and Agencia Nacional de Promoción Científica y Tecnológica (ANPCyT, PICT 2015-2651, PICT-2016-2908 and PICT-2018-1415) of Argentina.

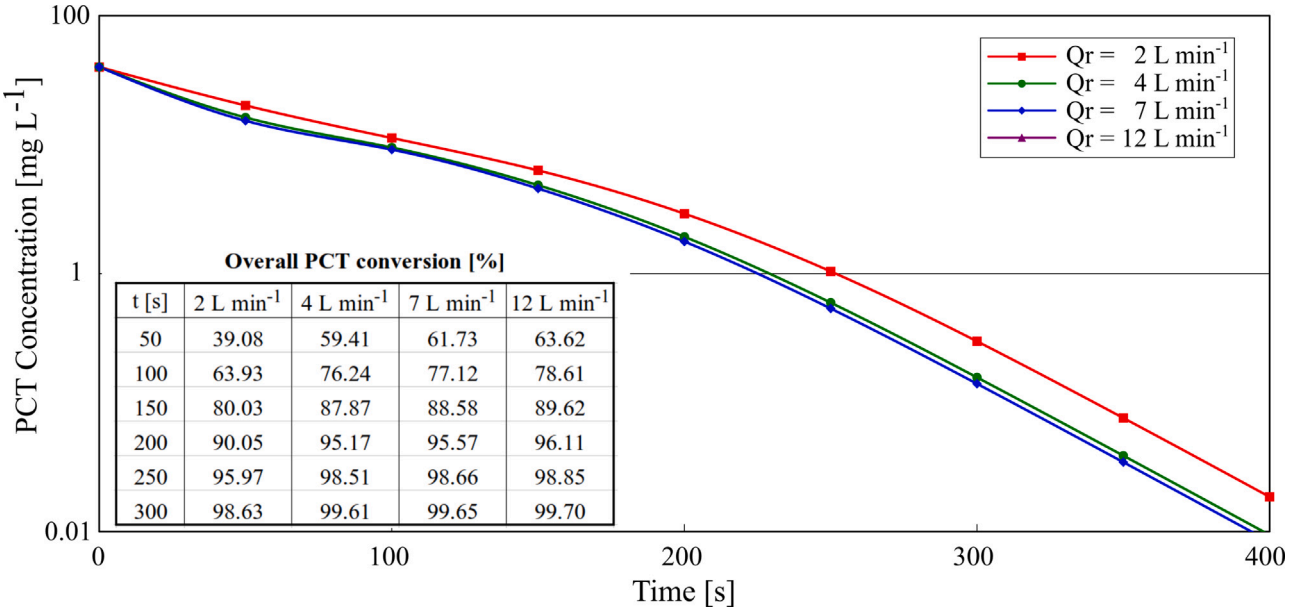

Overall PCT conversion [%]

t [s]	2 L min^{-1}	4 L min^{-1}	7 L min^{-1}	12 L min^{-1}
50	39.08	59.41	61.73	63.62
100	63.93	76.24	77.12	78.61
150	80.03	87.87	88.58	89.62
200	90.05	95.17	95.57	96.11
250	95.97	98.51	98.66	98.85
300	98.63	99.61	99.65	99.70

Fig. 12. Temporal evolution of the volume-averaged PCT on the system for different recirculation flows using injection setup C for Fe^{+2} = 10 mg L^{-1} and H_2O_2 = 94.5 mg L^{-1}.

References

[1] P. Zhang, H. Zhou, K. Li, X. Zhao, Q. Liu, D. Li, G. Zhao, Occurrence of pharmaceuticals and personal care products, and their associated environmental risks in a large shallow lake in north China, Environ. Geochem. Health 40 (4) (2018) 1525–1539, http://dx.doi.org/10.1007/s10653-018-0069-0.

[2] Y.-Y. Yang, J.-L. Zhao, Y.-S. Liu, W.-R. Liu, Q.-Q. Zhang, L. Yao, L.-X. Hu, J.-N. Zhang, Y.-X. Jiang, G.-G. Ying, Pharmaceuticals and personal care products (PPCPs) and artificial sweeteners (ASs) in surface and ground waters and their application as indication of wastewater contamination, Sci. Total Environ. 616 (2018) 816–823, http://dx.doi.org/10.1016/j.scitotenv.2017.10.241.

[3] S.Y. Wee, A.Z. Aris, F.M. Yusoff, S.M. Praveena, Occurrence and risk assessment of multiclass endocrine disrupting compounds in an urban tropical river and a proposed risk management and monitoring framework, Sci. Total Environ. 671 (2019) 431–442, http://dx.doi.org/10.1016/j.scitotenv.2019.03.243.

[4] R.R.Z. Tarpani, A. Azapagic, Life cycle environmental impacts of advanced wastewater treatment techniques for removal of pharmaceuticals and personal care products (PPCPs), J. Environ. Manag. 215 (2018) 258–272, http://dx.doi.org/10.1016/j.jenvman.2018.03.047.

[5] A. Ferrer-Aguirre, R. Romero-González, J.M. Vidal, A.G. Frenich, Simple and quick determination of analgesics and other contaminants of emerging concern in environmental waters by on-line solid phase extraction coupled to liquid chromatography–tandem mass spectrometry, J. Chromatogr. A 1446 (2016) 27–33, http://dx.doi.org/10.1016/j.chroma.2016.04.009.

[6] C.M. Manaia, J. Rocha, N. Scaccia, R. Marano, E. Radu, F. Biancullo, F. Cerqueira, G. Fortunato, I.C. Iakovides, I. Zammit, et al., Antibiotic resistance in wastewater treatment plants: tackling the black box, Environ. Int. 115 (2018) 312–324, http://dx.doi.org/10.1016/j.envint.2018.03.044.

[7] H.N.P. Vo, G.K. Le, T.M.H. Nguyen, X.-T. Bui, K.H. Nguyen, E.R. Rene, T.D.H. Vo, N.-D.T. Cao, R. Mohan, Acetaminophen micropollutant: Historical and current occurrences, toxicity, removal strategies and transformation pathways in different environments, Chemosphere 236 (2019) 124391, http://dx.doi.org/10.1016/j.chemosphere.2019.124391.

[8] E.S. Fisher, S.C. Curry, Evaluation and treatment of acetaminophen toxicity, Adv. Pharmacol. 85 (2019) 263–272, http://dx.doi.org/10.1016/bs.apha.2018.12.004.

[9] D. Kanakaraju, B.D. Glass, M. Oelgemöller, Advanced oxidation process-mediated removal of pharmaceuticals from water: a review, J. Environ. Manag. 219 (2018) 189–207, http://dx.doi.org/10.1016/j.jenvman.2018.04.103.

[10] A.R.L. Ribeiro, N.F. Moreira, G.L. Puma, A.M. Silva, Impact of water matrix on the removal of micropollutants by advanced oxidation technologies, Chem. Eng. J. 363 (2019) 155–173, http://dx.doi.org/10.1016/j.cej.2019.01.080.

[11] A. Gallego-Schmid, R.R.Z. Tarpani, S. Miralles-Cuevas, A. Cabrera-Reina, S. Malato, A. Azapagic, Environmental assessment of solar photo-fenton processes in combination with nanofiltration for the removal of micro-contaminants from real wastewaters, Sci. Total Environ. 650 (2019) 2210–2220, http://dx.doi.org/10.1016/j.scitotenv.2018.09.361.

[12] V.A. Paiva, C.E. Paniagua, I.A. Ricardo, B.R. Gonçalves, S.P. Martins, D. Daniel, A.E. Machado, A.G. Trovó, Simultaneous degradation of pharmaceuticals by classic and modified photo-fenton process, J. Environ. Chem. Eng. 6 (1) (2018) 1086–1092, http://dx.doi.org/10.1016/j.jece.2018.01.013.

[13] P. Soriano-Molina, J.G. Sánchez, S. Malato, P. Plaza-Bolanos, A. Agüera, J.S. Pérez, On the design and operation of solar photo-Fenton open reactors for the removal of contaminants of emerging concern from WWTP effluents at neutral pH, Appl. Catal. B: Environ. 256 (2019) 117801, http://dx.doi.org/10.1016/j.apcatb.2019.117801.

[14] S. Foteinis, J.M. Monteagudo, A. Durán, E. Chatzisymeon, Environmental sustainability of the solar photo-Fenton process for wastewater treatment and pharmaceuticals mineralization at semi-industrial scale, Sci. Total Environ. 612 (2018) 605–612, http://dx.doi.org/10.1016/j.scitotenv.2017.08.277.

[15] J. Martínez-Costa, J. Rivera-Utrilla, R. Leyva-Ramos, M. Sánchez-Polo, I. Velo-Gala, A. Mota, Individual and simultaneous degradation of the antibiotics sulfamethoxazole and trimethoprim in aqueous solutions by Fenton, Fenton-like and photo-Fenton processes using solar and UV radiations, J. Photochem. Photobiol. A: Chem. 360 (2018) 95–108, http://dx.doi.org/10.1016/j.jphotochem.2018.04.014.

[16] S. Malato, P. Fernández-Ibáñez, M.I. Maldonado, J. Blanco, W. Gernjak, Decontamination and disinfection of water by solar photocatalysis: recent overview and trends, Catal. Today 147 (1) (2009) 1–59, http://dx.doi.org/10.1016/j.cattod.2009.06.018.

[17] L.O. Conte, A.V. Schenone, O.M. Alfano, Ferrioxalate-assisted solar photo-Fenton degradation of a herbicide at pH conditions close to neutrality, Environ. Sci. Pollut. Res. 24 (7) (2017) 6205–6212, http://dx.doi.org/10.1007/s11356-016-6400-3.

[18] P. Soriano-Molina, J.G. Sánchez, O.M. Alfano, L.O. Conte, S. Malato, J.S. Pérez, Mechanistic modeling of solar photo-Fenton process with Fe^{3+}-EDDS at neutral pH, Appl. Catal. B 233 (2018) 234–242, http://dx.doi.org/10.1016/j.apcatb.2018.04.005.

[19] E.O. Marson, V.A. de Paiva, B.R. Gonçalves, O.G. Júnior, W.B. Neto, A.E. Machado, A.G. Trovó, Degradation of Direct Red 81 mediated by Fenton reactions: multivariate optimization, effect of chloride and sulfate, and acute ecotoxicity assessment, Environ. Sci. Pollut. Res. 24 (7) (2017) 6176–6186, http://dx.doi.org/10.1007/s11356-016-6977-6.

[20] A.A. Nogueira, B.M. Souza, M.W. Dezotti, R.A. Boaventura, V.J. Vilar, Ferrioxalate complexes as strategy to drive a photo-FENTON reaction at mild pH conditions: a case study on levofloxacin oxidation, J. Photochem. Photobiol. A: Chem. 345 (2017) 109–123, http://dx.doi.org/10.1016/j.jphotochem.2017.05.020.

[21] L.O. Conte, A.V. Schenone, B.N. Giménez, O.M. Alfano, Photo-Fenton degradation of a herbicide (2, 4-D) in groundwater for conditions of natural pH and presence of inorganic anions, J. Hazard. Mater. 372 (2019) 113–120, http://dx.doi.org/10.1016/j.jhazmat.2018.04.013.

[22] M.E. Farshchi, H. Aghdasinia, A. Khataee, Heterogeneous Fenton reaction for elimination of Acid Yellow 36 in both fluidized-bed and stirred-tank reactors: Computational Fluid Dynamics versus experiments, Water Res. 151 (2019) 203–214, http://dx.doi.org/10.1016/j.watres.2018.12.011.

[23] K. Tong, L. Yang, X. Du, Y. Yang, Review of modeling and simulation strategies for unstructured packing bed photoreactors with CFD method, Renew. Sustain. Energy Rev. 131 (2020) 109986, http://dx.doi.org/10.1016/j.rser.2020.109986.

[24] M. Bagheri, M. Mohseni, Pilot-scale treatment of 1, 4-dioxane contaminated waters using 185 nm radiation: experimental and CFD modeling, J. Water Process Eng. 19 (2017) 185–192, http://dx.doi.org/10.1016/j.jwpe.2017.06.015.

[25] F. Montecchio, M. Altimira, A. Andersson, K. Engvall, Fluid dynamics modelling of UV reactors in advanced oxidation processes for VOC abatement applications, Chem. Eng. J. 369 (2019) 280–291, http://dx.doi.org/10.1016/j.cej.2019.03.094.

[26] A. Dutta, N. Das, D. Sarkar, S. Chakrabarti, Development and characterization of a continuous solar-collector-reactor for wastewater treatment by photo-Fenton process, Sol. Energy 177 (2019) 364–373, http://dx.doi.org/10.1016/j.solener.2018.11.036.

[27] J. Moreno-SanSegundo, C. Casado, J. Marugán, Enhanced numerical simulation of photocatalytic reactors with an improved solver for the radiative transfer equation, Chem. Eng. J. 388 (2020) 124–183, http://dx.doi.org/10.1016/j.cej.2020.124183.

[28] H.G. Weller, G. Tabor, H. Jasak, C. Fureby, A tensorial approach to computational continuum mechanics using object-oriented techniques, Comput. Phys. 12 (6) (1998) 620–631.

[29] M. Dong, J. Cui, M. Jia, Y. Shang, S. Li, Large Eddy simulation of plasma-assisted ignition and combustion in a coaxial jet combustor, Energy (2020) 117463, http://dx.doi.org/10.1063/1.168744.

[30] H. Song, Y. Lin, X. Han, D. Yang, C. Zhang, C.-J. Sung, et al., The thermoacoustic instability in a stratified swirl burner and its passive control by using a slope confinement, Energy 195 (C) (2020) http://dx.doi.org/10.1016/j.energy.2020.117463.

[31] X. Han, D. Laera, D. Yang, C. Zhang, J. Wang, X. Hui, Y. Lin, A.S. Morgans, C.-J. Sung, Flame interactions in a stratified swirl burner: Flame stabilization, combustion instabilities and beating oscillations, Combust. Flame 212 (2020) 500–509, http://dx.doi.org/10.1016/j.combustflame.2019.11.020.

[32] E. Yamal-Turbay, E. Ortega, L.O. Conte, M. Graells, H.D. Mansilla, O.M. Alfano, M. Pérez-Moya, Photonic efficiency of the photodegradation of paracetamol in water by the photo-Fenton process, Environ. Sci. Pollut. Res. 22 (2) (2015) 938–945, http://dx.doi.org/10.1007/s11356-014-2990-9.

[33] F. Audino, L.O. Conte, A.V. Schenone, M. Pérez-Moya, M. Graells, O.M. Alfano, A kinetic study for the Fenton and photo-Fenton paracetamol degradation in an annular photoreactor, Environ. Sci. Pollut. Res. 26 (5) (2019) 4312–4323, http://dx.doi.org/10.1007/s11356-018-3098-4.

[34] G. Dalgic, I.F. Turkdogan, K. Yetilmezsoy, E. Kocak, Treatment of real paracetamol wastewater by Fenton process, Chem. Ind. Chem. Eng. Q. 23 (2) (2017) 177–186, http://dx.doi.org/10.2298/CICEQ150831029D.

[35] L.R. Rad, M. Irani, H. Pourahmad, M.S. Sayyafan, I. Haririan, et al., Simultaneous degradation of phenol and paracetamol during photo-Fenton process: Design and optimization, J. Taiwan Inst. Chem. Eng. 47 (2015) 190–196, http://dx.doi.org/10.1016/j.jtice.2014.10.014.

[36] A.C. Reina, L.S.-J. Jordá, J.G. Sánchez, J.C. López, J.S. Pérez, Modelling photo-Fenton process for organic matter mineralization, hydrogen peroxide consumption and dissolved oxygen evolution, Appl. Catal. B: Environ. 119 (2012) 132–138, http://dx.doi.org/10.1016/j.apcatb.2012.02.021.

[37] DOGC num. 3894, 2003, DECRET 130/2003, URL http://www.gencat.cat/diari/3894/03127147.

[38] R.F.P. Nogueira, M.C. Oliveira, W.C. Paterlini, Simple and fast spectrophotometric determination of H_2O_2 in photo-Fenton reactions using metavanadate, Talanta 66 (1) (2005) 86–91, http://dx.doi.org/10.1016/j.talanta.2004.10.001.

[39] ISO 6332: Water Quality - Determination of Iron - Sprectrometric Method Using 1, 10-Phenanthroline, International Organization for Standardization, 1988.

[40] S.V. Patankar, D.B. Spalding, A calculation procedure for heat, mass and momentum transfer in three-dimensional parabolic flows, in: Numerical Prediction of Flow, Heat Transfer, Turbulence and Combustion, Elsevier, 1983, pp. 54–73, http://dx.doi.org/10.1016/0017-9310(72)90054-3.

[41] R.I. Issa, Solution of the implicitly discretised fluid flow equations by operator-splitting, J. Comput. Phys. 62 (1) (1986) 40–65, http://dx.doi.org/10.1016/0021-9991(86)90099-9.

[42] A.E. Cassano, C.A. Martin, R.J. Brandi, O.M. Alfano, Photoreactor analysis and design: Fundamentals and applications, Ind. Eng. Chem. Res. 34 (7) (1995) 2155–2201, http://dx.doi.org/10.1021/ie00046a001.

[43] J.R. Howell, M.P. Menguc, R. Siegel, Thermal Radiation Heat Transfer, CRC Press, 2010.

[44] Y. Boyjoo, M. Ang, V. Pareek, Some aspects of photocatalytic reactor modeling using computational fluid dynamics, Chem. Eng. Sci. 101 (2013) 764–784, http://dx.doi.org/10.1016/j.ces.2013.06.035.

[45] H.A. Irazoqui, J. Cerdá, A.E. Cassano, Radiation profiles in an empty annular photoreactor with a source of finite spatial dimensions, AIChE J. 19 (3) (1973) 460–467, http://dx.doi.org/10.1002/aic.690190307.

[46] O.M. Alfano, R.L. Romero, A.E. Cassano, Radiation field modelling in photoreactors—I. Homogeneous media, Chem. Eng. Sci. 41 (3) (1986) 421–444, http://dx.doi.org/10.1016/0009-2509(86)87025-7.